Transmission electron microscopy and atomic force microscopy analysis of Nb-Al-AlOx-Nb superconducting tunnel junction detectors

N. Rando,[a] P. Videler, A. Peacock, A. van Dordrecht, and P. Verhoeve
Astrophysics Division, Space Science Department of the European Space Agency, ESTEC, Noordwijk, The Netherlands

R. Venn
Cambridge Microfab, Cambridge, United Kingdom

A. C. Wright
Advanced Materials Research Laboratory, MRIC, North East Wales Institute, Mold Road, Wrexham LL11 2AW, United Kingdom

J. Lumley
Oxford Instruments, Scientific Research Division, Cambridge, United Kingdom

(Received 27 June 1994; accepted for publication 4 January 1995)

The performance of photon detectors based on superconducting tunnel junctions are related to their current - voltage (I-V) curve characteristics and, ultimately, to the quality of the thin tunnel barriers (of order 1 nm) which separate the two superconducting thin films. Both the optimization of the spectroscopic performance of these detectors and the development of a reproducible and high yield fabrication route, require a better understanding of barrier quality and growth techniques. Transmission electron microscopy (TEM) and atomic force microscopy (AFM) provide valuable tools for the investigation of the barrier region and for the control of the quality of the different thin films and related interfaces. In this paper, the results of a TEM and AFM evaluation of Nb-Al-AlOx-Nb tunnel junctions are reported, together with their interpretation on the basis of the I-V curve performance at low temperature ($T \geqslant 0.3$ K). Thickness disuniformities of the Al plus AlOx overlayer and evidence of barrier defects have been found, which may place constraints on the spectroscopic performance of such devices. Through the use of TEM it has also been possible to confirm the epitaxial nature of the Nb base electrode. The junction counter electrode however appears to be polycrystalline, with a columnar morphology and an average grain width of 40 nm. The overall structure of the various layers may well place constraints on the tunneling characteristics of the device.

I. INTRODUCTION

Superconducting tunnel junction detectors (STJ's) are currently under extensive investigation because of their very good theoretical energy resolution. At x-ray energies (6 keV, $\lambda = 0.2$ nm) the number of charge carriers produced in a superconducting film by photoabsorption is of order $10^6 - 10^7$, i.e., about 1000 times higher than in a semiconductor detector, thereby accounting for the predicted improvement in energy resolution. A photon of energy γ produces a number of charge carriers $N_o = \gamma/\epsilon$, where ϵ is the mean energy required to create a single charge carrier. The predicted intrinsic full width at half maximum (FWHM) resolution of the detector is then $R_o(\text{eV}) = 2.355\sqrt{F\epsilon\gamma}$, where F is the Fano factor. In niobium, theoretical models indicate $F = 0.22$ and $\epsilon = 2.64$ meV, or $\epsilon = 1.74\Delta$, where Δ is the band gap of the superconductor.[1] This then corresponds to $R_o = 4.4$ eV at $\gamma = k$ 6 eV. A detailed description of the photoabsorption process and of the related quasiparticle production in a STJ are beyond the aim of this paper and can be found elsewhere.[1,2]

The performance of Nb-Al-AlOx-Nb or Nb-Al-AlOx-Al-Nb STJ's have been found to be related to the properties of their I-V curves, with particular regard to the subgap current, at bias voltages $V \ll 2\Delta/e$ and at temperatures of order one tenth the critical temperature T_c. The optimum operating conditions are given by low subgap currents (often referred to as thermal currents), which ensure higher dynamic resistances and which allow better signal to noise ratio during the detection of the excess current produced by the photoabsorption event (in contrast to the thermal current of the junction). In addition to an improved noise performance, subgap currents which decrease with the temperature are symptomatic of better quality films and more uniform insulating barriers, both essential qualities for improved spectroscopic performance. According to the standard BCS theory, at low temperature the subgap current is expected to decrease, because of its dependence on the quasiparticle number density, as $e^{-\Delta/kT}$. In the case of an ideal *SIS* junction (symmetric device) at low temperature ($kT \ll eV$), the predicted net current flowing across the tunnel barrier is the following:[3]

$$I_{SIS} = \frac{2}{eR_N}\int_{\Delta}^{\infty} \rho(E)\rho(E+eV)[f(E)-f(E+eV)]dE, \tag{1}$$

where $\rho(E) = E/\sqrt{E^2-\Delta^2}$ is the BCS density of states, $f(E) = (1+e^{E/kT})^{-1}$ is the Fermi function and E is the en-

[a]Electronic mail: nrando@astro.estec.esa.nl

 0021-8979/95/77(8)/4099/8/$6.00

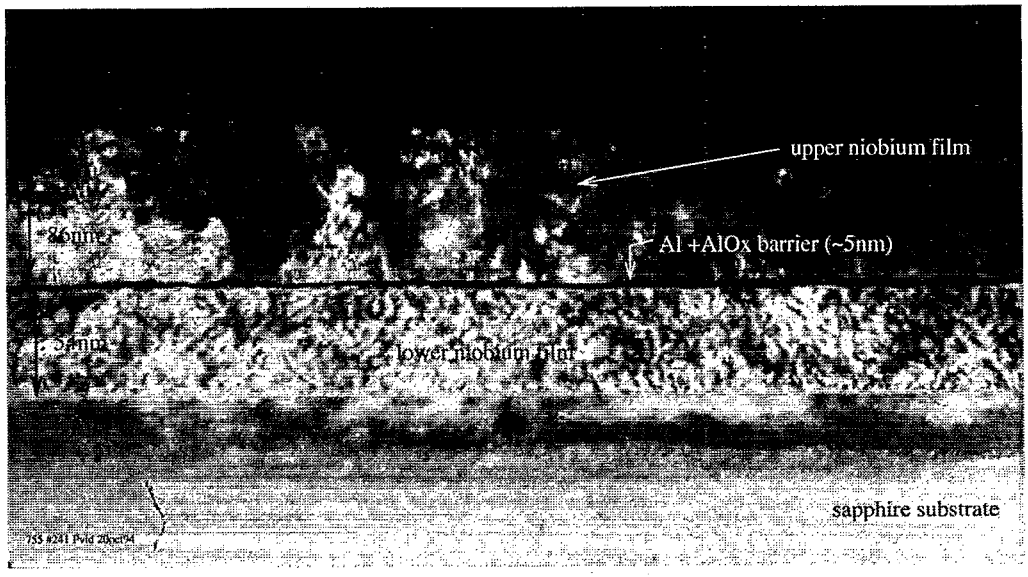

FIG. 1. Cross-sectional TEM image of the complete Nb-Al-AlOx-Nb junction multilayer. The measured thickness values are also indicated.

ergy of the quasiparticle charge carriers. At voltages $V>\Delta/2e$ the expression (1) can be approximated to read:

$$I_{th}(V,\Delta,T)=\frac{\rho(\Delta+eV)}{eR_N}\sqrt{2\pi kT\Delta}\;\; e^{-\Delta/kT}. \qquad (2)$$

Here R_N is the junction normal resistance. For $V<2\Delta/e$ the thermal current is only slowly varying with the bias voltage V. The major effort in the fabrication of high quality Nb based STJ's has therefore focused on the reproducible production of devices, with subgap currents decreasing with the operating temperature according to Eq. (2). In practice, the fabrication of such devices is affected by reproducibility issues and low yields, while the subgap current - temperature dependence stops at $T\leqslant 1$K, due to the presence of an additional leakage current I_L (c.f. Sec. III). The causes of these effects are believed to be related to disuniformities of the thin oxide layer which constitutes the tunnel barrier. Given the extremely low thickness (~ 1 nm), which is required for high conductance, the tunneling behavior of charge through these structures is dependent on both the granularity of the relevant interfaces (Al-AlOx-Nb) and spatial variations in the actual barrier thickness. The morphology of the thin films and their crystalline structure will also play an important role in the definition of the barrier characteristics. Spatial disuniformities at grain level are expected not only to affect the temperature dependence of the subgap current, but also to constrain the quasiparticle diffusion properties, so as to possibly degrade the energy resolution of these detectors.

In this paper we report the results obtained from a combined TEM and AFM inspection of both the barrier region and the film morphology of highly transmissive Nb-Al-AlOx-Nb junctions deposited on a smooth sapphire substrate.

II. JUNCTION FABRICATION AND AFM DATA

The development of a reliable procedure for the fabrication of high quality Nb-Al-AlOx-Nb has become of extreme interest for the improvement of STJ's as well as for a full exploitation of Josephson integrated circuits.[4] Most work has concentrated on the use of niobium because of the existence of a well established technology for the deposition of refractory, thermally recyclable thin films. Moreover, the critical temperature of niobium ($T_c=9.25$ K for bulk Nb) ensures relatively high operating temperatures (of order 1.2 K), an issue of clear importance for any future practical application.

The results reported here refer to samples produced from an original sandwich of Nb-Al-AlOx-Nb, deposited on a highly polished 13.5×7.5 mm and 0.5 mm thick sapphire substrate (R-plane orientation). A number of AFM (atomic force microscope) inspections carried out on the substrates showed their extremely high smoothness, with surfaces virtually featureless and imperfections at atomic level. Average roughness values (Ra) below 0.2 nm were recorded over sampling lengths of order 1 μm on the surface side of the substrate.

The complete trilayer sandwich is deposited with a single pump-down in an UHV chamber at a base pressure of about 2×10^{-9} Torr by means of a dc magnetron sputtering system. The base Nb film is grown first, epitaxially, with its a-axis almost perpendicular to the substrate plane. In this case the nominal thickness corresponds to 54 nm. A number of similar samples have been examined after the Nb base electrode deposition by means of x-ray diffraction analysis (Weissenberg technique) and they have been found to be epitaxial. This result has been also confirmed by a TEM analysis. At this stage it was not possible to ascertain the smoothness of the first epitaxial Nb layer.

After deposition of the Nb base, a 5 nm thick Al layer is deposited: this is a crucial step in the device fabrication, since a uniform Al coverage of the Nb base film is essential for achieving the required barrier quality. Any defect or disuniformity of the Al layer will in fact translate into an uneven AlOx barrier and therefore affect the device perfor-

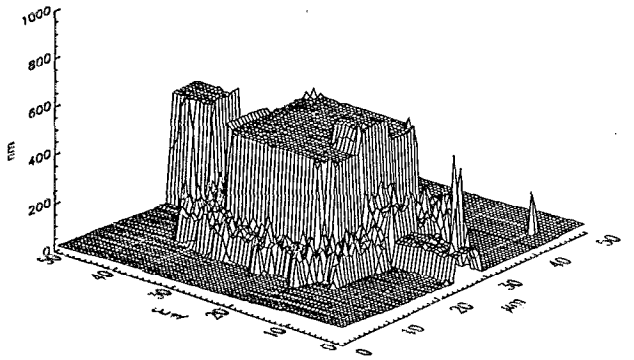

FIG. 2. AFM image of the surface heights of a 20 μm junction.

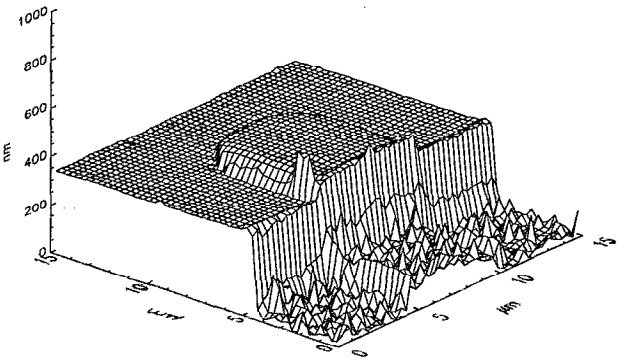

FIG. 3. The AFM image of the surface heights of the top film and lead of the 20 μm device shown in Fig. 2.

mance. The AlOx barrier is produced by thermal oxidation of the Al layer. Detailed measurements performed on equivalent devices indicate an estimated barrier thickness of 0.7–1.0 nm.[5]

Finally, a polycrystalline Nb top film of 86 nm was deposited on the AlOx barrier to form the junction counter-electrode. Figure 1 shows the TEM cross section of the complete multilayer including the Nb-sapphire interface. The Nb film thickness values measured from the TEM data are in good agreement with the expected values based on the calibration of the deposition system.

The samples used for the TEM analysis were obtained from unprocessed trilayer structures deposited over the complete substrate area. Several complete STJ's were also produced from the original trilayers by using a modified version of the SNEP process.[6] This has allowed a direct comparison between the current-voltage characteristics of the devices and the evaluation of the TEM and AFM images. In order to fabricate distinct junctions, the trilayer deposition is followed by a preliminary wet etch which defines the device geometry. This step is then followed by a plasma etch (RIE), which allows the further definition of the top electrode at the junction boundary (Nb-AlOx interface). After the RIE procedure, the device edges are anodized in order to allow a proper connection of the junction electrodes. An ion-milling of the the top film surface is performed before depositing the counter-electrode lead. Depending on the photolithographic mask geometry, eight square devices are fabricated on each chip, with areas ranging from 12×12 to 50×50 μm. Typical lead widths correspond to 3–5 μm. Figure 2 shows the AFM image of an equivalent 20 μm device. The enhanced roughness of the area of the base electrode not covered by the top film ("underlap") is due to the combined effect of the reactive ion etching and the successive anodization procedure. In particular, the anodization step is certainly responsible for a degradation of the surface smoothness due to the oxide formation. Inspection of Fig. 2 shows the top Nb film surface to be more uniform, with a Ra of order 1.5 nm. Figure 3 illustrates the surface profile in a high magnification AFM image of the top film and counter-electrode.

III. THE JUNCTION I-V CHARACTERISTICS

The results reported in this paper have been obtained from devices characterized by highly transmissive barriers, with critical current densities of order 500 A/cm^2. These barrier characteristics arise from the fact that STJ's require short tunneling times in order to maximize the charge output and, as a result, improve the energy resolution.[2] Such high critical current densities do however imply a severe requirement on the barrier quality. Important information on the barrier characteristics can be obtained by the analysis of the device I-V curve and in particular by monitoring the subgap current as a function of the temperature.[1] It is worth noting that a detailed analysis of the I-V curve of similar devices, also with highly transmissive barriers, has revealed the presence of subgap structures at $V=\Delta/e$ and $V=2\Delta/3e$. These structures can be interpreted as due to multiple particle tunneling (MPT). This process can only occur as a result of the highly transmissive nature of the barrier. While a thorough interpretation of these results can be found in Foden *et al.*,[5] it is important to stress that the presence of MPT structures indicates not only very thin barriers but that disuniformities across the device in the barrier thickness are to be expected.

The I-V data are acquired by means of a very low noise and low frequency unit, based on a 16 bit ADC-DAC scheme and on an electronically compensated two wire technique. The current-voltage curve is scanned in current, while the corresponding voltage is directly measured. The system allows high resolution measurements in the mA to pA range. In order to reveal the subgap current details, a magnetic field parallel to the junction films of order of ~ 100 Gauss is constantly applied. Accurate measurements have been performed by means of a 3 He system, down to 0.3 K, with the aim to monitor the behavior of the subgap current as a function of the temperature. The results are represented in Fig. 4 for various bias voltages. Note the tunnel current is reduced by about five orders of magnitude by decreasing the temperature between 2.2 and 0.8 K.[7] The different curves in Fig. 4 refer to currents measured at different bias voltages, below the $2\Delta/e$ point and outside any Fiske step region. The solid lines are the best fit curves of the form:

$$I_{subgap}(V,\Delta,T)=I_{th}(V,\Delta,T)+I_L(V), \tag{3}$$

where $I_{th}(V,\Delta,T)$ is given by Eq. 2 and $I_L(V)$, is an additional temperature independent leakage current. This leakage current $I_L(V)$, which is strongly dependent on the bias voltage V dominates at $T<1.0$ K. At temperatures higher than

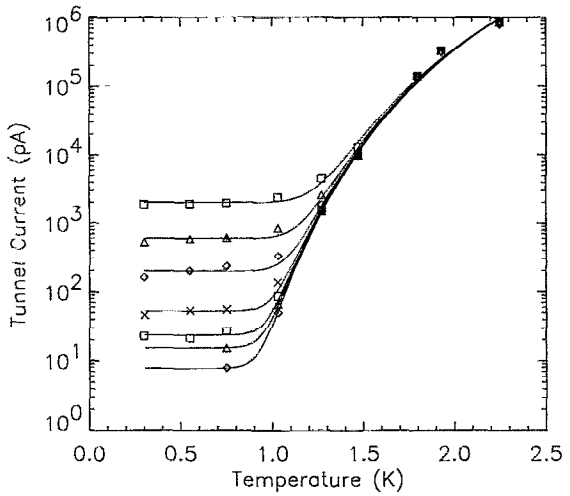

FIG. 4. Sub-gap current as a function of temperature at different bias voltages, ranging from Vb=0.2 mV to Vb=0.8 mV (0.1 mV steps) for a 20 μm device. Note the leakage current densities are as low as $J_L=0.05$ pA/μm^2

1.5–1.8 K and for $V<1$ mV the junction shows a nearly ideal BCS behavior. The presence of such a leakage current limits the ability of the junction to accurately measure the small excesses in charge carriers produced as a result of the absorption of a photon say in the Nb film. Such a leakage current must be related to either the presence of barrier disuniformities or perimeter anodization problems. We expect the absolute value of I_L to decrease with increasing barrier quality (lower defect density). Figure 5 shows the dependence of the leakage current $I_L(V)$ as a function of the bias voltage V. This dependence can be interpreted as the I-V characteristic associated with the barrier defects which may be observed in high resolution TEM images (c.f. Sec. IV).

While a more quantitative analysis of $I_L(V)$ as function of the bias voltage V cannot be presented at this stage, it is important to notice the strong non-linearity of this I-V characteristic. Barrier defects could be represented by areas having a much reduced AlOx thickness or even small regions in which the AlOx barrier is replaced by formation of Nb oxides. This is typically the case for a nonuniform coverage of the Nb base electrode by the Al overlayer, prior to the barrier oxidation. The oxidation of Nb is known to be particularly differentiated, producing various species, of which NbO has metallic properties.[8] In this case we could envisage the presence of a "parallel" current leakage mechanism characterized by an ohmic behavior, often referred to as "microshort" locations. The presence of a non-linear I-V leakage characteristic implies that other conduction mechanisms must be involved. We should also note that the presence of NbO may cause a band gap reduction in the adjacent Nb (by the proximity effect), potentially introducing further disuniformities in the detector response.

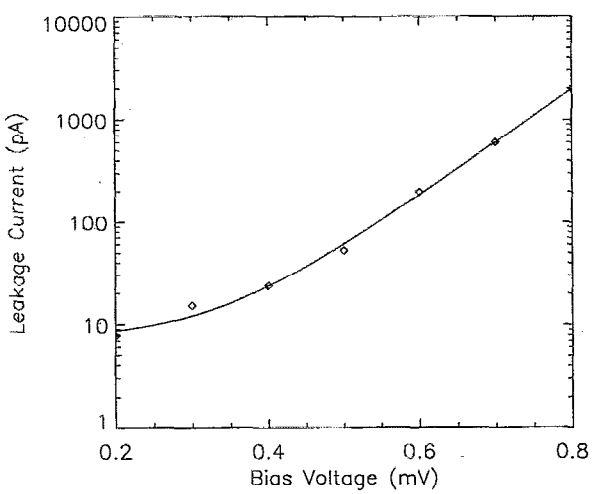

FIG. 5. Variation of the leakage current with the bias voltage. The best fit to a simple model of the form $I_{leak}=a+be^{cV}$ is also shown (where $a=7.2$ pA, $b=0.13$ pA, and $c=12.0$ mV^{-1}).

The high resolution TEM image analysis presented in Sec. IV aims to identify the causes of this leakage current by inspecting the barrier area and the related Nb film interfaces. The evaluation of these results, combined with the I-V curve interpretation, should in fact assist in the improvement of the fabrication procedure of Nb based superconducting tunnel junctions.

IV. THE TEM DATA

A. TEM sample preparation

Two pieces of the sample under test, approximately 4 mm by 2 mm were cut from the device using a peripheral saw fitted with a diamond wheel. These were then bonded together with the junction (layer) sides facing each other using high strength epoxy adhesive. To achieve a strong bond, the layer side of both pieces was lightly scratched with a diamond scriber away from the center of the sections. This was found to be necessary as non-scratched material tended to debond during later processing steps. To achieve a thin (<1 μm) glue line by a reduction in the viscosity, the epoxy adhesive was cured at 120 °C. The bonded pair was then trimmed down to approximately 2.5 mm by 2 mm, again by using the peripheral saw. The shorter dimension was then reduced further to a 40 μm thick section using a dimpling tool with diamond paste. A flat composite blank was prepared in this way rather than with one concave face as it was then possible to bond this directly to a 3 mm molybdenum specimen grid before removal from the dimpler specimen plattern. In this way very thin sections could be prepared with minimal risk of breakage during handling. These blanks were then thinned to electron transparency by argon-ion milling. Briefly, the details are incidence angle of 10 degrees, accelerating voltage of 5 keV and 60 μA of current per gun. Perforation took place after approximately 25 hours after which the ion-beam voltage was reduced to 4 keV for 5 minutes in order to reduce surface damage.

The specimen was examined at 300 keV on a Philips EM430T transmission electron microscope using both diffraction contrast and phase contrast imaging modes. For the latter mode, the instrument has a point resolution limit of 0.23 nm.

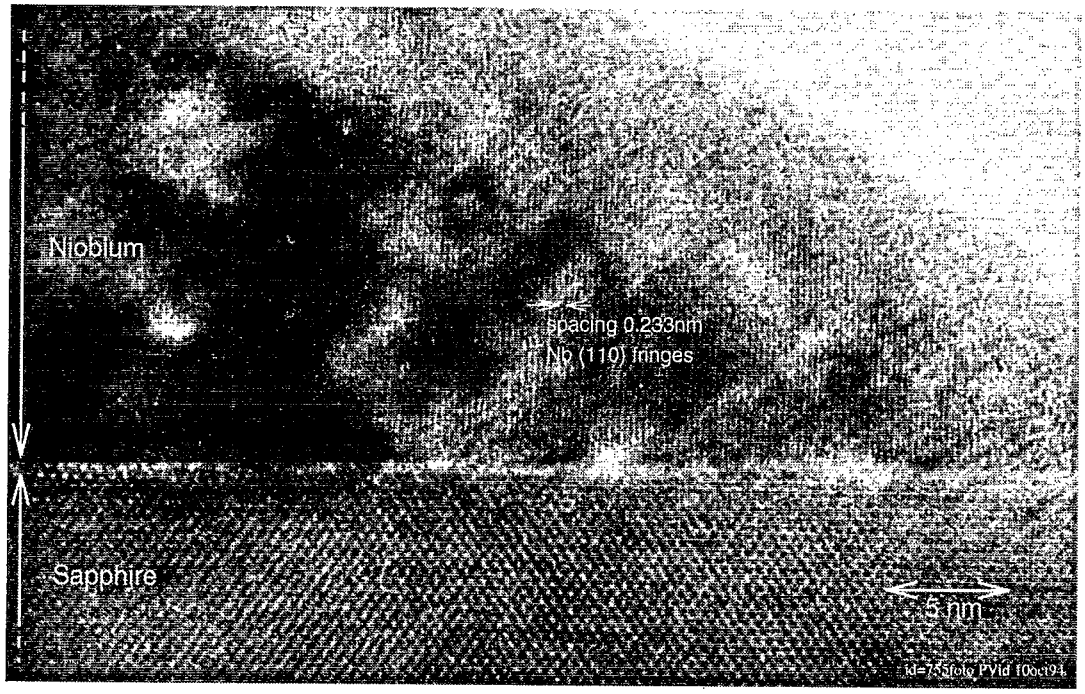

FIG. 6. Cross-sectional TEM image of the interface between the epitaxial Nb base film and the sapphire substrate. The lattice fringe spacings of both Nb and sapphire are clearly visible.

B. Results from the TEM tests

Initial examination of the cross-section confirmed that the sample had three layers grown onto the sapphire substrate as shown in Fig. 1 where the thin barrier layer can clearly be seen.

Selected area electron diffraction revealed that the lower Nb layer is epitaxial. In fact the [100] Nb is found to be parallel to the [1-102] sapphire and the [011] Nb and the [-111] sapphire are misoriented by 3.1 degrees.

By contrast, it was possible to determine that the upper Nb layer was polycrystalline with a columnar grain structure; the typical grain size being ~ 40 nm in lateral extent. The image shown in Fig. 1 also reveals that the barrier layer (Al+AlOx) is not straight as a result of the top surface of the epitaxial Nb layer having an undulating nature. This may have serious consequences on device performance.

Examination of the specimen using phase contrast clearly revealed the [110] fringes (at 0.233 nm spacing) in

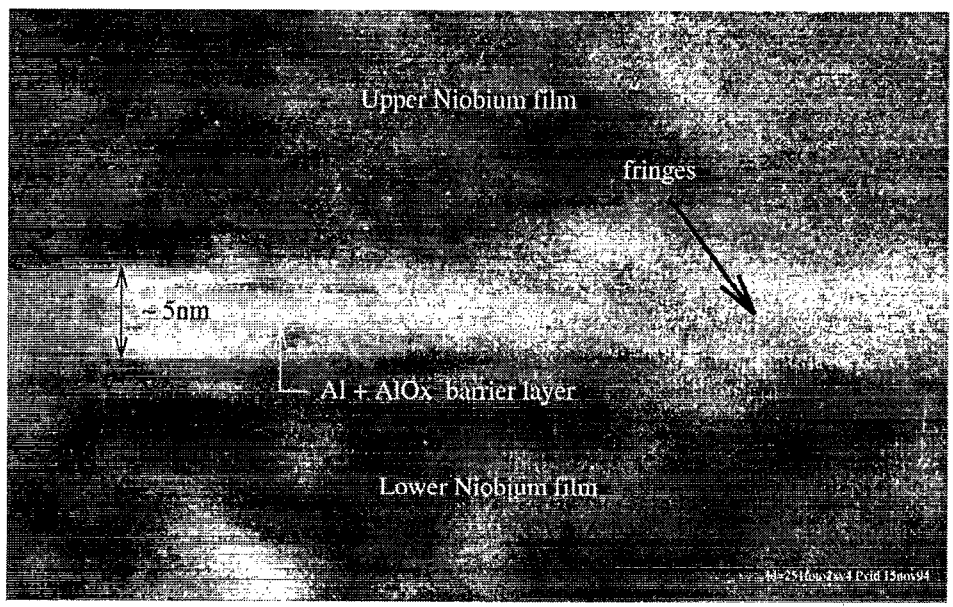

FIG. 7. High magnification cross-sectional TEM observation of the barrier layers (Al + AlOx). Lattice fringes similar to those from the lower epitaxial Nb layer are visible through the Al overlayer and are marked with an ↑ .

the Nb layers. Smaller lattice spacings in the Nb layers than these were not resolved. The [10-11] and [11-22] fringe spacings of the sapphire substrate were also clearly resolved. This is seen in Fig. 6 which shows the interface between the sapphire substrate and the epitaxial Nb layer. It is immediately apparent that the [110] fringes of the Nb layer are not precisely aligned to the substrate normal, being misaligned by some 2.5 degrees. In the case of silicon on sapphire, substrate steps have been cited as the cause of the slight misorientation of the epitaxial silicon layer.[9] The actual structure of the interface between the epitaxial Nb and the sapphire substrate cannot be ascertained from this image as there is insufficient resolution; other, smaller spatial frequencies would need to be resolved before this could be attempted using computer simulation methods.

Lattice imaging of the barrier layer (Al+AlOx) shows a granular appearance which is indicative of an amorphous structure. However, several parts of the barrier layer were found in which lattice fringes were seen to bridge the gap between the lower and upper Nb layers as seen in Fig. 7. Image processing of this region was used to compute the optical power spectrum of the image. Here, the spatial frequencies corresponding to the lattice fringes are marked and it can be seen that the fringes found within the barrier region are very similar in spacing to those from the lower epitaxial Nb layer. This may well be the origin of the "micro-shorts" and thus the leakage current shown in Fig. 5.

It is not possible from these images to say for certain whether there is any unoxidized aluminum adjacent to the lower Nb layer. The dark fringe visible at the top of the epitaxial Nb layer in some areas is not necessarily due to a change in composition: Fresnel fringe effects are often seen in high resolution electron micrographs where there are large changes in potential. Also, the effects of foil relaxation at edges and interfaces have to be considered which would lead to changes in local image intensity.

Further studies using dark field diffraction contrast imaging are underway to enhance the contrast from the unoxidized aluminum. The results will be reported in a future communication.

C. Image processing of the TEM data

The TEM images of the barrier region (Al+AlOx) have been processed further by means of a high resolution (2400 lines/mm) scanner with a 8 bit intensity scale. Using an 'edge finding' algorithm on the image we derived quantitative information on the Al+AlOx overlayer thickness distribution and on its longitudinal profile. Figure 8 shows a high resolution TEM image in which the interface with the Nb films is marked. In Fig. 9 the derived longitudinal profile of the Al-Nb film interfaces is plotted.

Significant variation in this Al+AlOx film thickness is observed with a typical overall spatial wavelength of ~40 nm, similar to the grain size of the Nb. Finer structure on much shorter wavelengths can also be observed. Note in general the Al and Nb top film interface profile is correlated with that of the Nb bottom film -Al interface profile. This implies that the surface profile of the epitaxial Nb film was not smooth prior to the deposition of the Al film. A peak to valley difference of as much as 5 nm can be easily observed.

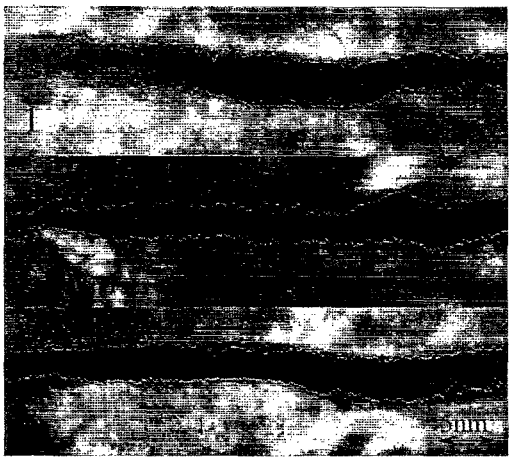

FIG. 8. High magnification cross-sectional TEM observation of the barrier layers (Al + AlOx). The sections marked 1–3 are the continuous image of the barrier region covering about 170 nm. The white dotted line indicate the interface profile determined by a computer edge finding algorithm.

The thickness variation of the Al+AlOx layer, as defined by the edge finding algorithm, has also been analyzed. The thickness distribution is shown in Fig. 10. A mean thickness of about 3.5 nm can be determined, with an associated standard deviation of around 0.7 nm.

Both from the barrier quality and detector performance point of view, the most important parameter is the thickness variation of the Al + AlOx layer: a strong variance on the thickness distribution could translate into a corresponding spatial variance of the barrier transmission characteristics. An extreme example is when the Al overlayer thickness is so much reduced as to substantially compromise the AlOx coverage, ultimately producing real barrier leakage. This possibility is actually reinforced by the inspection of Fig. 7, where some areas of the Al + AlOx layer present lattice fringes which are very similar to those of the epitaxial base film and which appear to bridge the two electrodes. Such features would clearly correspond to a defect in the insulating barrier.

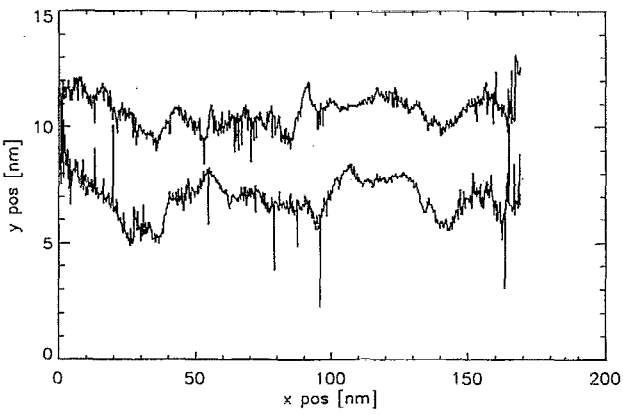

FIG. 9. Al + AlOx overlayer longitudinal profile as found with the edge finding algorithm of Fig. 8.

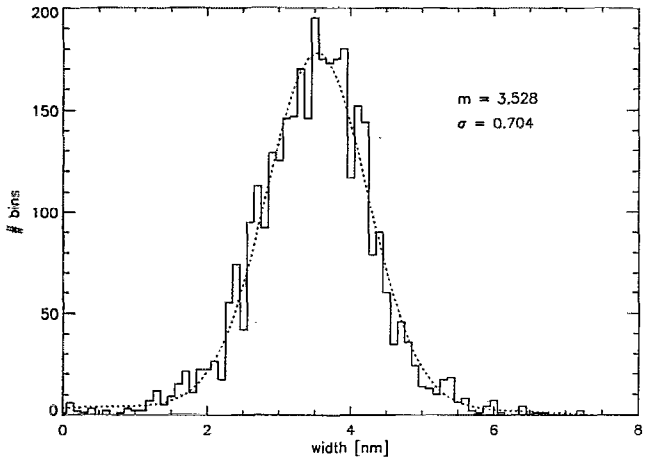

FIG. 10. Al + AlOx overlayer thickness distribution as measured from the cross-sectional TEM observations.

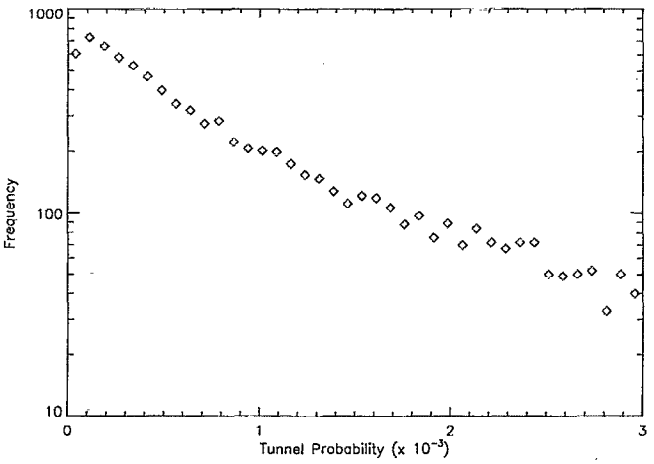

FIG. 11. Calculated frequency distribution of barrier tunnel probabilities for the case of 10 Å thick barrier with a relative thickness variance as described by that of Fig. 10.

Considering the smoothness of the substrate interface and the epitaxial growth of the base electrode, the interface between the base Nb and the Al overlayer presents a considerable waviness: this might be partly responsible for the overall thickness disuniformity of Al + AlOx and is one of the issues to be further investigated, both in terms of the diagnostic approach as well as the fabrication procedures. Possible causes could be related to the base electrode sputtering conditions. Recent investigations[4] have also shown that the Nb-Al interface roughness is increased further by annealing in a nitrogen ambient at 400 °C, due to Al-Nb boundary inter-diffusion effects. These effects are likely to be relevant when high temperature fabrication procedures are involved. In our case, all the examined samples were fabricated well below this temperature regime.

The measured thickness variations in the Al + AlOx overlayer and the presence of crystalline, bridging areas between base and top film, indicate a serious possibility of spatial variations in the actual AlOx barrier characteristics. The presence of spatial variations in the barrier transmissivity is a potential cause of degradation in the spectroscopic performance of the STJ. It could in fact introduce an additional variance on the detected charge on top of that expected from Fano charge fluctuations alone. It is in fact worth noting that a few percent variation in the AlOx barrier thickness translates into large changes in the tunneling probability.

For a single particle of mass m incident normal to a simple one dimensional rectangular potential barrier of thickness d and potential height ϕ relative to the Fermi level the tunneling probability can be simply written:

$$P_t \propto e^{(-2d/\hbar)\sqrt{2m(\phi-\Delta)}}. \tag{4}$$

If the observed relative variance in the Al+AlOx layer of $\sigma(d_{\mathrm{Al+AlOx}})/d_{\mathrm{Al+ALOx}}$ ~20% (Fig. 10) were of a similar order in the AlOx barrier, then major variations in the tunnel probability would exist (Fig. 11). For example based on Eq. (4), assuming ϕ~0.5 eV, P_t would follow an exponential frequency distribution with a mean and standard deviation for the tunnel probability of 8.5×10^{-4}. The effect of such a variation in tunnel probability on the spectroscopic performance of the detector is related to the quasiparticle (QP) diffusion process which takes place after the photoabsorption event. As it is well known, the quasiparticle diffusion length depends mainly on the thin film qualities, normally represented by the residual resistance ratio (RRR). It is important to note that the base electrode (epitaxial film) and counter-electrode (polycrystalline film) have very different RRR's: typical values are as high as 100 for high quality epitaxial films and of order 5–10 for lower quality, polycrystalline top films. In a first approximation we can use a simple QP transport model, based on a free electron assumption; in this case we find QP mean free paths Λ ranging from 15 nm (RRR=5) to 260 nm (RRR=100). Using these values to evaluate the diffusion constant at T=1.2 K and calculating the diffusion length over a typical event pulse duration (of order 500 ns) we find values comparable with the device dimensions (of order 20 μm for the top film and 80 μm for the epitaxial base electrode). If l is the typical junction dimension and Γ_{tun} the tunneling rate, we then find $l \simeq \sqrt{D/\Gamma_{tun}}$. Recent estimates, based on highly collimated x-ray illumination on samples similar to the ones subjected to TEM and AFM analysis,[10] indicate a QP diffusion length of about 26 μm for the base electrode lead.

Considering that these values are much larger than the observed barrier disuniformities, we would expect the diffusion process to overcome any mayor degradation related to a position dependent detector response. Nevertheless, highly collimated x-ray illumination experiments over 20 or 50 μm square devices,[11] have shown that the spectroscopic performance of STJD's are remarkably dependent on the photoabsorption site, within a few μm scale. Further investigations are underway, but preliminary indications, combined with results provided by low temperature scanning electron microscopy analysis,[12] seem to point in the direction of anisotropic QP diffusion and relevant edge effects.

It should be noted that the different film qualities of the base and counter-electrode translate into different tunneling probabilities as a consequence of different loss mechanisms. This factor plays an important role in the definition of the

statistical noise associated with tunneling in STJD's. For each film (i= 1 or 2) we can in fact write that the tunneling probability P_i is:[13]

$$P_i=\frac{\Gamma_{i,tun}}{\Gamma_{i,tun}+2\Gamma^*_{i,r}+\Gamma_{i,x}}, \tag{5}$$

where $\Gamma_{i,tun}$ is the tunneling rate, $\Gamma^*_{i,r}$ is the effective recombination rate and $\Gamma_{i,x}$ is a temperature independent loss rate. In the general case, where $P_1 \neq P_2$ and back-tunneling takes place, the tunneling statistical noise can exceed the Fano limited noise; moreover, as clearly stated in Ref. 13, any position dependence of Γ_{tun} or Γ_x is going to increase the signal variance.

No attempt here is made to predict the expected variance in the observed charge distribution based on such barrier thickness variations since the assumptions on the charge diffusion would dominate.

The TEM images have shown that the top Nb film is not only polycrystalline, with an average grain size of about 40 nm but that it is columnar in structure. Another hypothesis which is currently under investigation is the possibility of a reduced QP transmissivity across the grain boundaries. In this case the confinement of charge in a single grain would in fact enhance the quasiparticle number density and locally depress the order parameter. This effect would be equivalent to the formation of a trapping mechanism responsible for quasiparticles recombination and, in the end, for a reduced detector responsivity.[14] If this hypothesis was correct, the overall detector response from the top polycrystalline film would be represented by the superimposition of all the single grain contributions, with each grain showing its own charge confinement and tunneling properties. It is clear from x-ray collimation experiments that spatial variations over dimensions of below 10 μm are apparent.[15,10] The energy resolution of the overall detector would therefore reflect the variation in the average tunnel probability per grain. In such a case major improvements in the resolution of the top film may not then be observed unless the collimation was of the order of the grain size.

V. CONCLUSIONS

TEM and AFM represent indispensable techniques for the investigation of the thin tunnel barrier of Josephson devices and their thin film morphology. In particular, the capability of providing crystallographic information, make the TEM a very valuable tool for the development of reproducible fabrication procedures. The results provided by TEM inspections can be effectively complemented by the information deduced from the I-V characteristics of single devices and, in particular, with the analysis of the subgap current as a function of the temperature. Through this approach, it is possible to identify the most probable cause of the leakage current as being shorts through the thin barrier from the epitaxial base Nb film. A detailed series of measurements on Nb-Al-AlOx-Nb devices has shown the presence of thickness disuniformities in the Al+AlOx overlayer, as well as the evidence of possible bridging between the base and the counter electrode films in specific areas of the tunnel barrier. While AFM and also stylus measurements of the sapphire substrate material made in air, have shown a high degree of surface flatness over long ranges, the presence in the TEM images of surface steps at the epitaxial niobium to sapphire interface shows that there is a degree of crystallographic misorientation in the substrate material being used, and this misalignment may be a contributory factor in the marked topography seen at the epitaxial Nb-Al interface observed.

In addition the TEM images of the polycrystalline Nb top electrode indicate an average grain width of about 40 nm with a columnar type structure.

Finally, these results show how a close feed-back between deposition techniques, diagnostic activities, and device testing is clearly necessary in order to ensure the development of a mature technology in the field of Nb based STJ's. Such a technology is an indispensable basis for the improvement in the performance of superconducting tunnel junction detectors. It is in fact clear that their ultimate spectroscopic capabilities will be limited by the disuniformities of the barrier coupled to the charge diffusion properties of the films as well as by any charge trapping mechanism associated with the film morphology.

ACKNOWLEDGMENTS

The authors wish to thank Johnathan Howlett and Miles Wallis of Oxford Instruments /TFG (UK) for the actual fabrication of the devices as well as Jane Haycocks and Margared Stedman from National Physical Laboratory (UK) for the excellent AFM diagnostic work performed.

[1] N. Rando, A. Peacock, A. van Dordrecht, C. Foden, R. Engelhardt, B. Taylor, J. Lumley, and C. Pereira, Nucl. Instrum. Methods A **313**, 173 (1992).
[2] N. Rando, A. Peacock, C. Foden, A. van Dordrecht, J. Lumley, and C. Pereira, J. Appl. Phys. **73**, 5098 (1993).
[3] N. Booth, P. Brink, R. Gaitskell, D. Goldie, A. Hahn, G. L. Salmon, and A. Swift, J. Low Temp. Phys. **93**, 521 (1993).
[4] S. Morohashi and S. Hasuo, Appl. Phys. Lett. **63**, 2285 (1993).
[5] C. Foden, N. Rando, A. van Dordrecht, A. Peacock, J. Lumley, and C. Pereira, Phys. Rev. B **47**, 3316 (1993).
[6] M. Gurvitch, M. Washington, H. Huggings, and J. Rowell, IEEE Trans. Magn. **19**, 791 (1983).
[7] P. Hübner, N. Rando, A. Peacock, P. Videler, A. van Dordrecht, and J. Lumley, Proc. SPIE **2006**, 308 (1993).
[8] J. Halbritter, Appl. Phys. A **43**, 1 (1987).
[9] R. C. Pond, M. Aindow, C. Dineen, and T. Peters, in *Epitaxial Growth of (001)Si on Vicinal (01-12) Sapphire*, Oxford University (IOP, Bristol, 1987), Vol. 87.
[10] P. Verhoeve, N. Rando, P. Videler, A. van Dordrecht, A. Peacock, R. Venn, and D. Goldie, Proceedings of the Workshop on Superconductivity and Particle Detection, Toledo, 1994.
[11] P. Verhoeve, N. Rando, P. Videler, A. van Dordrecht, A. Peacock, A. van Dordrecht, D. Goldie, J. Lumley, J. Howlett, M. Wallis, and R. Venn, Proceedings of the SPIE conference, San Diego, 1994.
[12] J. le Grand, M. P. Bruijn, C. Patel, P. de Korte, S. Lemke, R. Gross, and R. P. Huebener, Proceedings of the Workshop on Superconductivity and Particle detection, Toledo, 1994.
[13] D. Goldie, P. Brink, C. Patel, N. Booth, and G. Salmon, Appl. Phys. Lett. **64**, 3169 (1994).
[14] D. van Vechten and K. S. Wood, Phys. Rev. B **43**, 12852 (1991).
[15] P. Videler, N. Rando, A. Peacock, P. Hübner, and A. van Dordrecht, J. Low Temp. Phys. **93**, 587 (1993).